Lambertian surfaces with over- and under-filled field of view

Nathaniel Field, Joseph Shaw

Nathaniel J. Field, Joseph A. Shaw, "Lambertian surfaces with over- and under-filled field of view," Proc. SPIE 12213, Optics Education and Outreach VII, 1221309 (3 October 2022); doi: 10.1117/12.2633738

SPIE.

Event: SPIE Optical Engineering + Applications, 2022, San Diego, California, United States

Lambertian surfaces with over- and under-filled field of view

Nathaniel J. Field[a], Joseph A. Shaw[*a,b]

[a]Electrical & Computer Engineering Dept., Montana State University, Bozeman, MT USA 59717
[b]Optical Technology Center, 334 NAH, Montana State University, Bozeman, MT USA 59717

ABSTRACT

Optical science and engineering education and practice make frequent use of the concepts of Lambertian surfaces, Lambertian reflectance, or Lambertian emission. These are all based on Lambert's cosine law, which states that the radiant or luminous intensity [W/sr] reflected or emitted from a Lambertian surface varies as the cosine of the angle between the direction of incident (or emitted) radiation and the surface normal. However, a simpler definition is a Lambertian source produces radiance [W/(m^2 sr)] that is constant with angle. This definition helps avoid common errors and confusion that arise when a Lambertian source is viewed in different geometries in which the field-of-view (FOV) solid angle is over- or under-filled by the source. In this paper we describe the theory of Lambertian reflection and emission for under- and over-filled FOV situations and show measurements from a simple set of reflection experiments that help to prove these theories in practice by demonstrating that flux measured with an under-filled FOV varies as the cosine of the viewing angle, while flux measured with an over-filled FOV does not. We also show how to set up and conduct experiments to illustrate these different situations using a simple halogen lamp, lens, photodiode, and Lambertian panel.
Keywords: Lambertian, radiometry, reflection, scattering, emission

1. INTRODUCTION

Optical science and engineering education and practice make frequent use of the concepts of Lambertian surfaces, Lambertian reflectance, or Lambertian emission. These are all based on Lambert's cosine law, which states that the radiant or luminous intensity $[W/sr]$ reflected or emitted from a Lambertian surface varies as the cosine of the angle between the direction of incident (or emitted) radiation and the surface normal. However, this definition is too often erroneously applied to other radiometric or photometric quantities that do not necessarily follow the cosine pattern, or to the "signal" generically. The meaning is clarified when Lambertian reflection or emission is described as having equal radiance $[W/m^2sr]$ at all angles. While many textbooks do reference this definition directly at some point in the discussion of diffuse surfaces,[1-4] they tend to leave out discussion of the influence of viewing geometry, which may lead to later confusion and misattribution. The most common unnoted assumption when discussing Lambertian surfaces is that the observer or detector has a sufficient field of view (FOV) to fully encompass the Lambertian surface at normal incidence. When this assumption does not hold true, the derived formulas describing the observed flux are no longer accurate. Such situations are common in remote sensing imaging, for example, when the instantaneous FOV (iFOV) for a single pixel tends to contain only a small fraction of a viewed Lambertian surface.

With the constant-radiance definition of Lambertian, the optical flux incident on a detector is found by multiplying the radiance emitted or reflected from the surface (which is constant with angle) by the throughput for the sensor system and the surface being measured. This throughput is proportional to the product of an area and a projected solid angle that opens away from that area. For example, the area is often the entrance pupil area, in which case the solid angle is determined by the FOV (or iFOV for a multi-pixel system) or the size and distance of the Lambertian surface, whichever is smaller. In other words, which solid angle should be used depends on whether the detector FOV is over- or under-filled by the source. In this paper, we will derive the formulas describing the detected flux for both geometries and provide data and procedures for simple laboratory demonstrations.

*joseph.shaw@montana.edu; phone 1 406-994-7261; https://www.montana.edu/jshaw/

Optics Education and Outreach VII, edited by G. Groot Gregory,
Anne-Sophie Poulin-Girard, Proc. of SPIE Vol. 12213, 1221309
© 2022 SPIE · 0277-786X · doi: 10.1117/12.2633738

2. LAMBERTIAN THEORY FOR REMOTE SENSING

We begin by defining Lambertian as having constant radiance $[W/m^2 sr]$ over all angles and areas. While most texts begin with Lambert's cosine law and then derive constant radiance, we do the reverse. Though Lambertian can be used to describe an emitting or reflecting source, we describe the theory from a general source perspective. In a reflection geometry, both the angle of illumination θ_i and the viewing angle θ_v are relevant to the reflected power. For the source case, only θ_v applies. The theories discussed still apply to the equivalent scenario of a Lambertian reflector with a fixed θ_i, to the inverse scenario of a reflector with fixed θ_v and varied θ_i, and to the complex situation of a reflective geometry with simultaneously varying θ_i and θ_v.

First, we must define the two possible geometries: under-filled and over-filled. In an under-filled geometry, the projected solid angle subtended by the source projected area as seen from the receiver, Ω_s, is less than the receiver FOV projected solid angle, Ω_{FOV}; otherwise, the geometry is over-filled. This is illustrated for a simple case in Fig. 1, which shows a basic receiver with Ω_{FOV} defined by the chief rays (solid lines) extended backward from the outer edges of the detector (field stop) through the center of the lens (aperture stop) and Ω_s defined by rays from the outer edges of the source extending forward through the center of the lens (dashed lines). When Ω_s and Ω_{FOV} are matched, you might refer to the geometry as critically filled, but it behaves the same as an over-filled geometry.

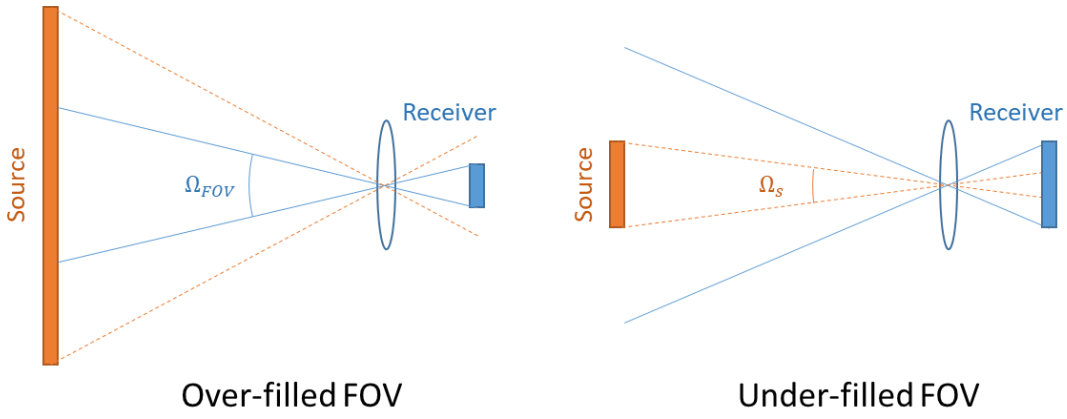

Figure 1. Diagram of a simple receiver (lens and detector) for both over-filled and under-filled geometries.

Consider an infinitely large Lambertian surface viewed by a receiver with a finite FOV; this results in an over-filled geometry for all viewing angles. In this geometry, the flux $[W]$ at the detector, Φ_d, is equal to the radiance of the target times the throughput of the receiver:

$$\Phi_d = L_s A_{ep} \Omega_{FOV}, \tag{1}$$

where A_{ep} is the area of the lens in a simple system (or the entrance pupil of a more complex receiver) and L_s is the radiance of the source. Since all values in Eq. 1 are constant for any viewing angle, the detected flux does not depend on the viewing angle θ_v.

However, real sources are finite and will therefore produce a projected area $[A_p = A * \cos(\theta_v)]$ that becomes smaller than Ω_{FOV} at some viewing angle θ_v. For sources with solid angles Ω_s much greater than Ω_{FOV}, this critical geometry viewing angle will be very near 90°, where practical viewing is impossible. But, for situations where the two solid angles are less than two orders of magnitude apart, the flux at the detector will decrease rapidly at viewing angles beyond the critical geometry angle. This effect can be seen clearly in the example in section 3.2.

The simplest situation is an under-filled geometry. Since Ω_s is less than Ω_{FOV} in this geometry, the flux on the detector is instead calculated using Ω_s, which is itself a function of the projected area of the source $A_{p,s}$, such that $\Phi_d \propto \Omega_s \propto A_{p,s} \propto \cos(\theta_v)$. More explicitly,

$$\Phi_d = L_s A_{ep} \frac{A_s * \cos(\theta_v)}{Z_{ep,s}^2}, \tag{2}$$

where $Z_{ep,s}$ is the distance between the lens (or entrance pupil) and the source. So long as the distance is held constant, all values in Eq. 2 other than θ_v are constant. From this, the source radiant intensity I_s $[W/sr]$ becomes

$$I_s = L_s A_s * \cos(\theta_v). \tag{3}$$

For a constant source, I_s varies only as a function of $\cos(\theta_v)$, which is an expression of Lambert's cosine law.

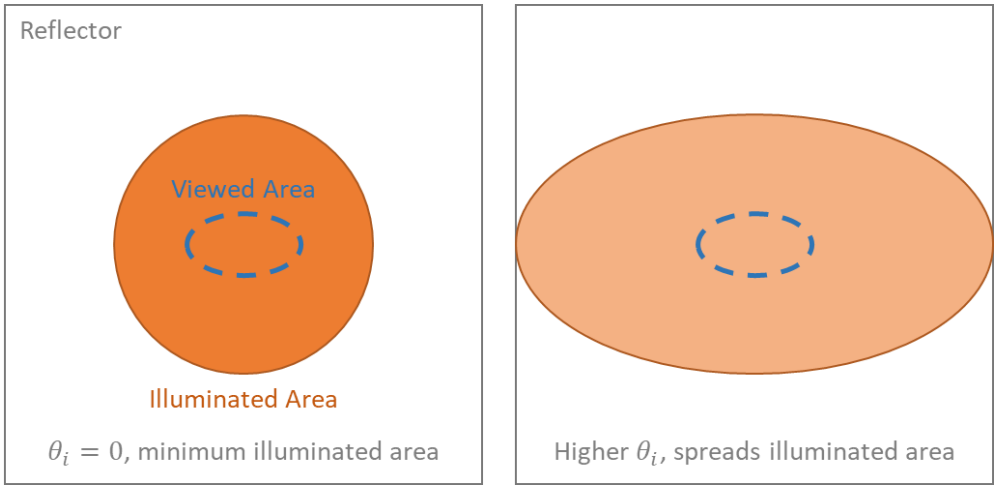

Figure 2. Illustration of a fixed θ_v with varying θ_i. The same amount of flux lies in the illuminated areas, but it is more dispersed across the spread area for a larger illumination angle θ_i.

Everything derived for this Lambertian source applies directly for a Lambertian reflector with a fixed illumination angle, θ_i. It also applies less intuitively and inversely for a Lambertian reflector with a fixed θ_v and varying θ_i. Figure 2 shows that for an over-filled FOV with a fixed viewing angle, as θ_i increases, the illuminated area increases as well, and assuming the illumination source has constant flux, Φ_s $[W]$, the reflector irradiance E_s $[W/m^2]$ must decrease as well. The Lambertian reflector radiance L_s $[W/m^2 sr]$ is a function of irradiance on the reflector surface as

$$L_s = \frac{\rho_s E_s}{\pi} = \frac{\rho_s \Phi_s \cos(\theta_i)}{\pi A_s}, \tag{4}$$

where ρ_s is the reflectance of the Lambertian surface π is the hemispheric projected solid angle into which the incident flux is diffused. When ρ_s, Φ_s, and A_s are constant for a given surface, we find that $L_s \propto E_s \propto \cos(\theta_i)$. In this situation, with an initially under-filled FOV, the limiting solid angle increases as a function of $\cos(\theta_i)$. Combined with decreasing radiance described above, detected flux, Φ_d, remains constant.

As a special aside, we can also consider the case of a monostatic remote sensing system, such as a lidar, for which the viewing and observation angles are always the same ($\theta_v = \theta_i$). Whether over- or under-filled, the limiting solid angle remains constant for the monostatic case. However, the radiance still decreases as a function of increasing illumination angle, $L_s \propto \cos(\theta_i)$.

3. LAB EXAMPLES AND PROCEDURES

Included here are two laboratory procedures for relatively simple setups that illustrate the importance of sensor-scene geometry in determining the response of a detector to a Lambertian surface. In both setups, we used a halogen lamp with a diffusing screen as the illumination source, a 5-cm square Spectralon® panel with nominal 99% reflectance as the reflecting surface, and a ThorLabs PDA10A2 silicon fixed-gain detector with a 25.4-mm biconvex lens for the receiver. The Lambertian reflector illuminated at a fixed angle behaved as a Lambertian source for these measurements.

Because we used a broadband detector in the visible range, we reduced secondary light sources during measurements – closing curtains and turning off room lights. If the background light is consistent over the measurement time, this isn't strictly necessary, as background primarily adds a DC offset to the detector voltage. However, Spectralon® does display a reflection function most similar to an ideal Lambertian reflector when illuminated or viewed at normal incidence, so the DC offset may include some minor dependance on viewing angle that cannot be easily compensated. This also informs lamp placement, as it should be as close to normal illumination as possible without casting shadows when the detector is at near-normal incidence.

3.1 Under-filled geometry

When taking measurements for an under-filled geometry, the biggest issue is typically getting a source that is small enough to fit within your FOV. When the source size is limited, you can increase the distance from the source to the receiver, $Z_{ep,s}$, to achieve $\Omega_s < \Omega_{FOV}$. However, if you must increase the lens-target distance, signal strength can be maintained by increasing it only so that $\Omega_{FOV} \gtrapprox 1.2 * \Omega_{targ}$, which for circularly symmetric source and FOV means the diameter of the area within the FOV at the source distance should be about 20% larger than the source diameter. For a different source shape, using the largest aspect (e.g., the length of the diagonal for a square target) helps to maintain an under-filled geometry while also mitigating the range-squared loss of flux falling on the detector. For our under-filled measurements (Fig. 3), we placed the lens 1.09 m from the source and 12.5 mm from the detector. This was the shortest achievable distance between lens and detector – providing the largest FOV with 2.3° half-angle – and the lens-target distance was chosen so that the diameter of the FOV area of the target was about 87 mm – 1.2 times the diagonal of the 5-cm square panel. A semi-circle with the origin at the target aided in keeping a fixed lens-target distance, and more easily denoted the angles at which we were measuring.

Figure 3. Setup for under-filled measurements. The necessary lens-source distance was greater than what could be achieved on our available optics benches, so we used a large area of a concrete lab floor. The post mounted behind the detector (red) was particularly

useful for use with an alignment mark on the back of the detector casing for angular alignment of the detector to the source at large distances. The illumination angle was approximately 30° in this setup.

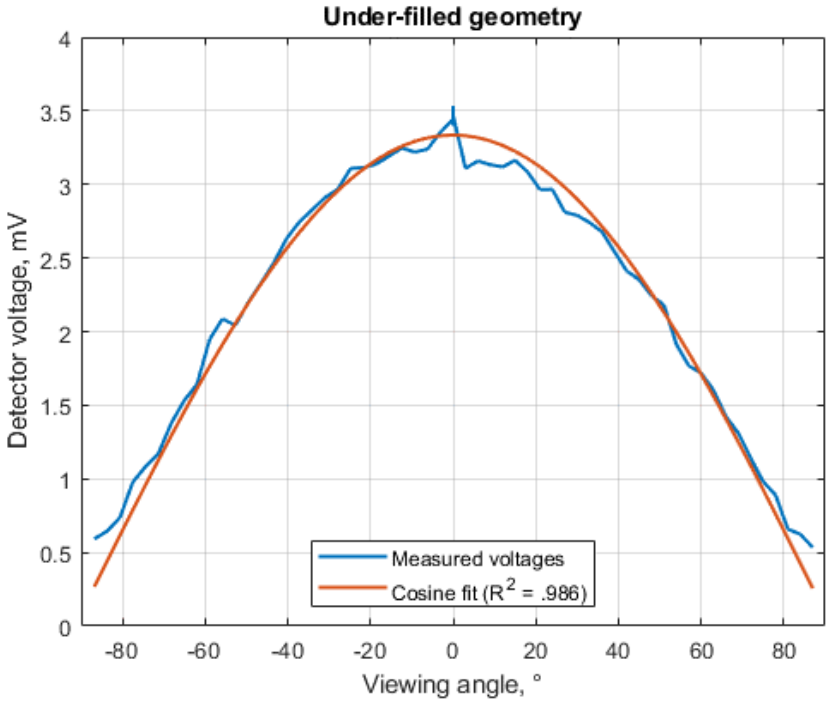

Figure 4. The results of our lab measurements for an under-filled geometry, showing both the voltages read from the detector (blue) and the fitted cosine function (red). The cosine shows strong correlation, with $R^2 = 0.986$.

The data collected from this setup are presented in Fig. 4, along with a fitted cosine with a fixed period (2π), fixed angular offset (0°), and fixed DC offset (0 mV). As expected for this geometry, the data closely match the fitted cosine. Some notable, but equally expected, features are the trends of the voltage signal to be slightly less than the fitted cosine for small viewing angles and slightly greater than the fitted cosine for large viewing angles. This is a well-established, small deviation of Spectralon® from an ideal Lambertian surface, which becomes more pronounced as the greater of the illumination or viewing angles increase.[5-8]

Also of note for this discussion is the vertical axis of Fig. 2. The "signal" typically referred to in papers is often a voltage, current, or digital number produced by the detector, though it is not always directly stated as such. While in this case we did see the signal (voltage) decrease as a function of $\cos(\theta_v)$, the more precise description is that the flux falling on the detector was decreasing with viewing angle because of the decreasing source solid angle caused by the projected source area. This is the physical phenomenon described by Lambert's cosine law or the alternate constant-radiance definition of Lambertian discussed in section 2.

3.2 Over-filled geometry

It can be much simpler to record measurements in the over-filled geometry, though issues can sometimes arise – primarily when the FOV is made too small and the flux falling on the detector is insufficient to overcome noise. For the most part, however, the physical nature of most lab equipment will lend more easily to this geometry.

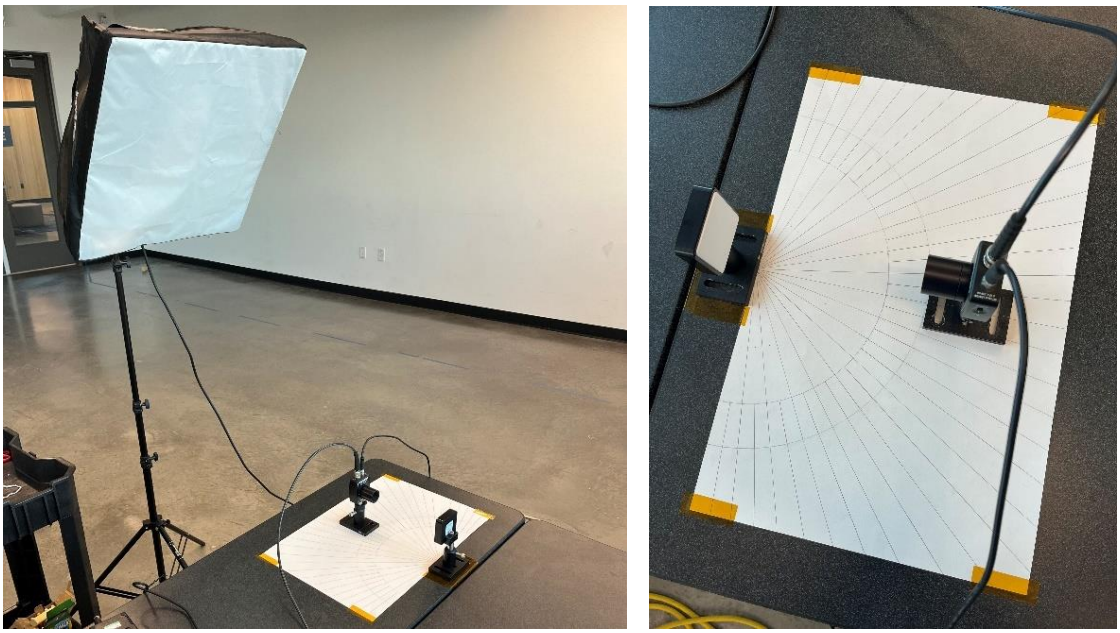

Figure 5. Lab setup for the over-filled geometry. The detector was much closer to the target, resulting in higher flux and improved signal-to-noise ratio despite viewing a much smaller fraction of the source area. The illumination angle was approximately 30° here.

For this setup, shown in Figure 5, we placed the lens 171 mm from the source and 12.5 mm from the detector, resulting in a 13.7-mm diameter of the viewed area on the source – meaning that only about 6% of the source area was viewed at normal incidence. Before taking measurements, it is useful to consider the critical geometry angle θ_{cg} at which the projected area of the FOV moves off the edges of the illuminated panel. The critical geometric angle can be calculated using the limiting dimension of the source d_s and the expanded dimension of the projected viewed area, d_{FOV}:

$$\theta_{cg} = \cos^{-1}\left(d_{FOV}/d_{targ}\right). \tag{5}$$

For our scenario, the limiting dimensions were the diameter of the viewed area at the target and the side-length of the square target, giving a critical angle of $\theta_{cg} = \cos^{-1}(13.7/50.8) \approx 74°$. This angle represents the viewing angle at which an ideal Lambertian surface would no longer produce a flat response, but a quick look at the measured results in Fig. 6 reveals a significant reduction of flux falling on the detector up to 15° closer to normal incidence.

The data displayed in Fig. 6 show a very poor correlation to a cosine function but do show a relatively flat response for viewing angles around normal incidence and out to about 60°. This is as expected for the over-filled geometry, but again we see some slight deviations from a perfectly flat response, which can be explained at least partially by the impossibility of an ideal Lambertian surface. For off-normal illumination, the reflection factor decreases with increasing θ_i;[5] however, the reflectivity increases with increasing θ_v when illuminated off-normal.[6,7] These two effects on reflectance in combination explain the slight dip in the center of the plot in Fig. 6, which then rises slightly before approaching the critical geometry and falling off.

For the steepest viewing angles, there is actually reasonable correlation to the cosine function fixed to the same parameters as those for the under-filled geometry's fit. A geometry with a smaller θ_{cg} would have more points with which to compare this outer edge cosine trend, but it is also unlikely that the fit would be particularly accurate except at the steepest θ_v, as the observed area does still increase as a function of the viewing angle, it just becomes more complex than a $\cos(\theta_v)$ relation (see Fig. 7). Even for our relatively simple circular FOV centered on a square target, the equation for the observed target area past the critical geometry becomes

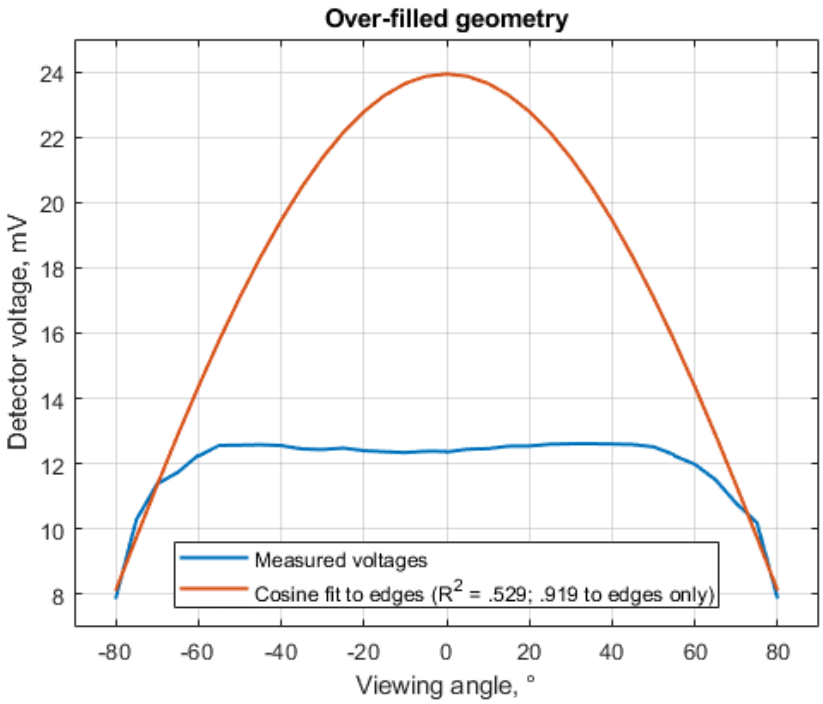

Figure 6. Lab measurements for an over-filled geometry, showing both the detector voltages (blue) and the fitted cosine function (red). The cosine shows poor correlation overall, which is to be expected as the over-filled geometry produces a relatively flat response for viewing angles from about -60° to 60°.

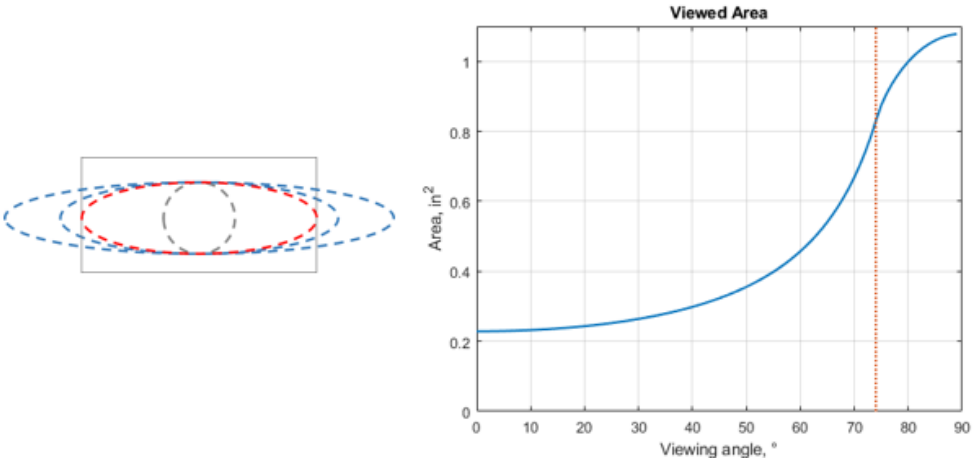

Figure 7. Depiction of the projected FOV on a source with straight edges (left) and a plot of the observed source area as a function of viewing angle (right) for our over-filled geometry. The condition where the critical geometry occurs is shown in red in both images. Note that the asymptotic maximum area is the initial diameter of the FOV area at the target multiplied by the width of the panel (1.37 cm × 5 cm ≈ 6.85 cm^2).

$$A_{obs} = \frac{d_{FOV}^2}{4\cos(\theta_v)}\left[\pi - 2\left(\cos^{-1}(h) - 2h\sqrt{h-h^2}\right)\right], \tag{6}$$

where

$$h = \frac{d_{targ}\cos(\theta_v)}{d_{FOV}}. \tag{7}$$

Ultimately, the over-filled geometry never truly shifts to an under-filled geometry by altering only illumination or viewing angles, but it does approach the under-filled scenario as the angles become increasingly steep.

4. SUMMARY AND CONCLUSIONS

We have discussed a definition of an ideal Lambertian surface as having constant radiance over all angles. We applied this definition to derive the classic Lambert's cosine law using a simple-to-complex conceptual approach, which may be more intuitive for students. We also underscored the importance of sensing geometry – particularly the distinction between an over- or under-filled FOV – with regard to the detected electrical signal at a detector from a Lambertian reflector or source. In short, for a fixed illumination angle, the over-filled scenario has constant flux at the detector (Φ_d), and the underfilled scenario has Φ_d which varies as the cosine of the viewing angle. For a fixed viewing angle, the under-filled scenario has constant Φ_d and the over-filled scenario has Φ_d which varies as the cosine of the illumination angle. For the special case of a monostatic system such as a lidar, Φ_d varies as the cosine of the incidence angle.

We also took special care to describe the physical phenomena regarding ideal diffuse surfaces with specific terms and units, so as to avoid generic "signal" terminology. We presented two brief laboratory experiments in sufficient detail to be repeated with simple optical lab equipment, which further emphasize the importance of understanding whether a receiver-target combination is in an over- or under-filled FOV case. These experiments also included discussion of important caveats and potential roadblocks which may arise with either scenario. We believe this approach to describing Lambertian surfaces and the subsequent cognizance of sensing geometry will benefit students of optics as well as those who must consider near-Lambertian reference surfaces for calibration of remote sensing systems.

Acknowledgment

This material is based upon work supported in part by the U.S. Air Force Research Laboratory via a subcontract through S2 Corp. with a fundamental research exemption.

References

[1] Bennett, C., [Principles of Physical Optics], John Wiley & Sons, Hoboken, NJ (2008).
[2] Pedrotti, F. L., Pedrotti, L. S., and Pedrotti, L. M., [Introduction to Optics, 3rd Ed.], Pearson Prentice Hall, Upper Saddle River, NJ (2007).
[3] Graham-Smith, F., King, T. A., and Wilkins, D., [Optics and Photonics: An Introduction, 2nd Ed.], John Wiley & Sons West Sussex, UK (2007).
[4] Dereniak, E. L. and Boreman, G. D., [Infrared Detectors and Systems], John Wiley & Sons, New York, NY (1996).
[5] Jackson, R. D., Clarke, T. R., and Moran, M. S., "Bidirectional calibration results for 11 Spectralon and 16 BaSO4 reference reflectance panels," Rem. Sens. Env. 40(3), 231-239 (1992).
[6] Georgiev, G. T. and Butler, J. J., "BRDF study of gray-scale Spectralon," Proc. SPIE 7081, 708107 (2008).
[7] Bhandari, A., Hamre, B., Frette, Ø., Zhao, L., Stamnes, J. J., and Kildemo, M., "Bidirectional reflectance distribution function of Spectralon white reflectance standard illuminated by incoherent unpolarized and plane-polarized light," Appl. Opt. 50(16), 2431–2442 (2011).
[8] Field, N. J., Brown, J. P., Card, D. B., Welsh, C. M., Van Rynbach, A. J., and Shaw, J. A., "Gray Spectralon polarized reflectance deviations from Lambertian," Proc. SPIE 12112, 121120A (2022).